TRPV1 pore turret dictates distinct DkTx and capsaicin gating

Matan Geron[a,1], Rakesh Kumar[a,1], Wenchang Zhou[b], José D. Faraldo-Gómez[b], Valeria Vásquez[c,2], and Avi Priel[a,2]

[a]The Institute for Drug Research, School of Pharmacy, Faculty of Medicine, The Hebrew University of Jerusalem, Ein Karem, 9112102 Jerusalem, Israel; [b]Theoretical Molecular Biophysics Laboratory, National Heart, Lung and Blood Institute, National Institutes of Health, Bethesda, MD 20892; and [c]Department of Physiology, The University of Tennessee Health Science Center, Memphis, TN 38163

Edited by Ramon Latorre, Universidad de Valparaíso, Valparaíso, Chile, and approved October 25, 2018 (received for review June 5, 2018)

Many neurotoxins inflict pain by targeting receptors expressed on nociceptors, such as the polymodal cationic channel TRPV1. The tarantula double-knot toxin (DkTx) is a peptide with an atypical bivalent structure, providing it with the unique capability to lock TRPV1 in its open state and evoke an irreversible channel activation. Here, we describe a distinct gating mechanism of DkTx-evoked TRPV1 activation. Interestingly, DkTx evokes significantly smaller TRPV1 macroscopic currents than capsaicin, with a significantly lower unitary conductance. Accordingly, while capsaicin evokes aversive behaviors in TRPV1-transgenic *Caenorhabditis elegans*, DkTx fails to evoke such response at physiological concentrations. To determine the structural feature(s) responsible for this phenomenon, we engineered and evaluated a series of mutated toxins and TRPV1 channels. We found that elongating the DkTx linker, which connects its two knots, increases channel conductance compared with currents elicited by the native toxin. Importantly, deletion of the TRPV1 pore turret, a stretch of amino acids protruding out of the channel's outer pore region, is sufficient to produce both full conductance and aversive behaviors in response to DkTx. Interestingly, this deletion decreases the capsaicin-evoked channel activation. Taken together with structure modeling analysis, our results demonstrate that the TRPV1 pore turret restricts DkTx-mediated pore opening, probably through steric hindrance, limiting the current size and mitigating the evoked downstream physiological response. Overall, our findings reveal that DkTx and capsaicin elicit distinct TRPV1 gating mechanisms and subsequent pain responses. Our results also indicate that the TRPV1 pore turret regulates the mechanisms of channel gating and permeation.

TRPV1 | DkTx | transgenic *C. elegans* | pore turret | capsaicin

Sensory neurons of the pain pathway (i.e., nociceptors) are excited by a multitude of plant and animal toxins that inflict pain (1). However, while some of these toxins produce this effect indirectly by causing tissue damage and the release of algogenic substances from nonneuronal cells, others directly elicit pain mainly by targeting membrane proteins selectively expressed by nociceptors (1–5). One of these membrane proteins, the transient receptor potential vanilloid 1 (TRPV1), is a nonselective cation channel activated by several plant and animal toxins, noxious heat, protons, and bioactive lipids such as anandamide and 15-HPETE (6–11). To date, TRPV1-activating animal toxins have been identified in venoms from centipedes, scorpions, snakes, and spiders (12–16). However, while the molecular basis of TRPV1 activation by the small molecule phytotoxins capsaicin and resiniferatoxin (RTX) has been extensively studied, the activation mechanism of TRPV1 by peptide animal toxins is not fully understood (17–20).

Vanillotoxins (VaTx) constitute a group of four spider peptide toxins that activate TRPV1 by interacting with the channel's outer pore region (12, 13, 21). Three of these toxins (VaTx1, VaTx2, and VaTx3) evoke reversible activation of TRPV1, whereas the fourth vanillotoxin, double-knot toxin (DkTx), produces a slowly developing and persistent activation of this channel (12, 13). Bohlen et al. (13) identified DkTx in venom of the Chinese bird spider (*Ornithoctonus huwena*), whose bite produces substantial pain and inflammation (22). This toxin has a unique bivalent structure which consists of two highly homologous inhibitory cysteine knot (ICK) motifs connected by a linker, bestowing the toxin its name (13).

As was shown in the structures obtained by cryo-EM and molecular dynamics simulations of the TRPV1–DkTx/RTX and TRPV1–DkTx complexes, respectively, the two ICK motifs of DkTx bind two homologous binding sites in adjacent subunits of the tetrameric channel, while its linker adopts a taut and constrained conformation (21, 23, 24). DkTx's ICKs also interact with lipids in the membrane bilayer, forming a toxin–channel–lipid tripartite complex (21). The toxin's antibody-like structure enables it to form a stable bond with TRPV1 and lock the channel in an open state; when separated, its single knots (K1 and K2) produce reversible channel activation similar to that evoked by other VaTxs (13, 25). The formation of a highly stable DkTx–TRPV1 complex was presumed to produce a maximal current amplitude, resulting in a debilitating and persistent pain response associated with the spider bite (13, 21, 25). However, the physiological aspects of TRPV1 activation by this toxin were yet to be examined. Moreover, although DkTx induces an essentially irreversible and stable TRPV1 activation, the macroscopic current amplitude evoked by this toxin is lower in comparison with currents elicited by this channel's reversible activators, such as capsaicin (13, 26). This phenomenon was observed in trigeminal neurons, heterologous expression systems such as HEK293 cells, and proteoliposomes containing purified TRPV1 channels (7, 13).

Significance

The TRPV1 channel integrates noxious stimuli from multiple sources to evoke an appropriate pain response. However, while different stimuli evoke distinct channel activation, the underlying molecular mechanisms remain unclear. Here, we aim at elucidating the structural determinants that regulate the different TRPV1 responses to two toxins: capsaicin and double-knot toxin (DkTx). We found that the channel pore turret domain imposes two opposite effects on the responses to these toxins. While it restricts the ion conductance of the DkTx-evoked current, it stabilizes the open channel state evoked by capsaicin. Together, our results indicate that TRPV1 pore turret dictates different gating mechanisms in response to agonists acting through different binding domains.

Author contributions: V.V. and A.P. designed research; M.G., R.K., W.Z., and V.V. performed research; M.G., W.Z., J.D.F.-G., V.V., and A.P. analyzed data; and M.G., V.V., and A.P. wrote the paper.

The authors declare no conflict of interest.

This article is a PNAS Direct Submission.

[1]M.G. and R.K. contributed equally to this work.

[2]To whom correspondence may be addressed. Email: vvasquez@uthsc.edu or avip@ekmd.huji.ac.il.

This article contains supporting information online at www.pnas.org/lookup/suppl/doi:10.1073/pnas.1809662115/-/DCSupplemental.

Published online November 21, 2018.

Here, we sought to elucidate the molecular mechanism underlying the unique, subdued TRPV1 activation by DkTx. We hypothesized that several structural elements in the toxin and the channel determine the unique activation profile induced by DkTx. First, by combining electrophysiological recordings (whole-cell and single channel) and behavioral analysis in transgenic *Caenorhabditis elegans*-expressing rat TRPV1 (rTRPV1), we show that DkTx locks TRPV1 in a subconductance state. Next, we engineered mutated toxins and channels to reveal the molecular determinants underlying the unique DkTx-evoked TRPV1 response. We found that when separated, each of the single knots that constitute the heteromeric bivalent DkTx evokes higher subconductance states than WT DkTx, while homomeric bivalent toxins (consisting of two identical knots, K1K1 and K2K2) evoke a DkTx-like subconductance. Importantly, we found that an engineered DkTx with an extended linker evokes higher conductance currents and more robust worms' aversive responses in comparison with the WT toxin. Likewise, deletion of the TRPV1 pore turret—a sequence of 23 aa protruding out of the outer pore region plain—abolishes the DkTx subconductance state and allows maximal current amplitude. Accordingly, the DkTx-evoked aversive response was dramatically potentiated in *C. elegans* expressing this truncated channel. Our analysis further revealed that the pore turret is essential for the allosteric coupling between the vanilloid binding pocket and the upper gate. In summary, our results demonstrate that DkTx evokes a distinct TRPV1 gating modality, which is mainly governed by the length of the toxin linker and the channel pore turret, potentially through steric hindrance. Thus, our findings indicate that the distinct activation of the pain pathway by DkTx and capsaicin is dependent on a unique TRPV1 gating mechanism.

Results

DkTx Produces Diminished TRPV1 Activation in Whole-Cell Recordings. While previous studies indicate that DkTx evokes subdued TRPV1 activation, the structural and functional aspects regarding this phenomenon remain unknown (7, 13, 21). Thus, we sought first to characterize DkTx-evoked TRPV1 activation in detail. To this end, recombinant DkTx was produced via periplasmic expression and purified using reversed-phase (C18) chromatography (*SI Appendix*, Fig. S1 *A* and *B*). The potency of recombinant DkTx to activate TRPV1 [EC_{50} = 0.11 ± 0.01 μM, Hill coefficient (n_H) = 1.5 ± 0.1] was comparable to that of venom-isolated toxin, as previously described (*SI Appendix*, Fig. S1*C*) (13).

Next, to determine the magnitude of DkTx-evoked TRPV1 activation, we employed the whole-cell configuration of the patch-clamp technique and recorded macroscopic currents evoked by the toxin and capsaicin in HEK293T cells stably expressing rTRPV1. In accordance with previous studies (13, 21, 25), DkTx evoked a slowly developing, outwardly rectifying, irreversible current featuring a reversal potential indistinguishable from the one measured with capsaicin (Fig. 1 *A* and *B*). Moreover, we found that the amplitude of this current was significantly lower at a saturating toxin concentration of 10 μM, compared with currents evoked by a saturating capsaicin concentration ($I_{DkTx}/I_{Capsaicin}$ = 55.9 ± 1.6%) (Fig. 1 *A* and *B*). Furthermore, this response is not species-specific, as comparably low DkTx-evoked current amplitudes were recorded in HEK293T cells expressing either human or rat TRPV1 (*SI Appendix*, Fig. S2*A*).

A possible explanation for the low TRPV1 current magnitudes evoked by DkTx is that the irreversible binding of this toxin imposes a distinct pore configuration compared with the one enforced by capsaicin. To test this possibility, we applied capsaicin together or after DkTx application. As shown in *SI Appendix*, Fig. S2*B*, coapplication of the two agonists induced current magnitudes comparable to those elicited by capsaicin alone. However, washing away the DkTx/capsaicin solution from the cells resulted in current amplitude levels similar to those obtained with the irreversible DkTx alone, indicating that both

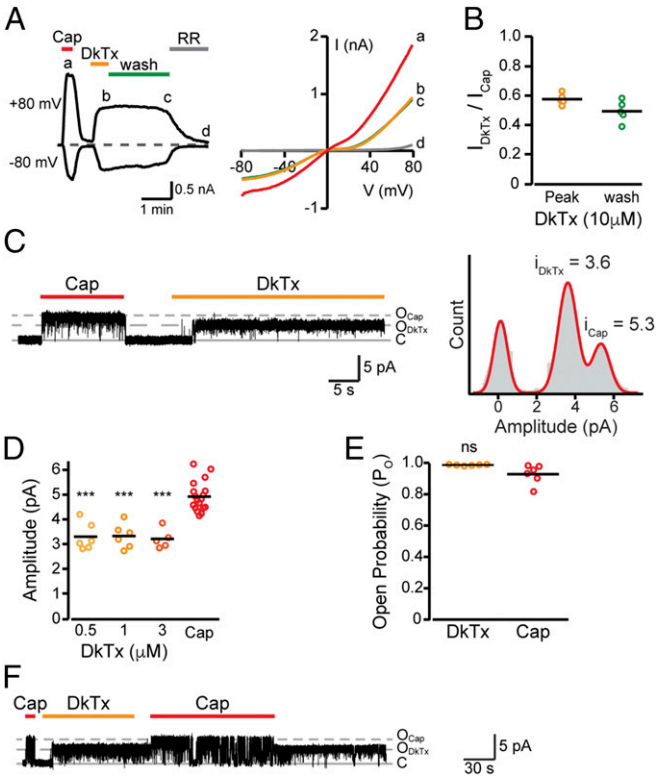

Fig. 1. DkTx evokes a moderate TRPV1 activation. (*A*, *Left*) Representative whole-cell current traces from TREx HEK293T cells stably expressing rTRPV1 at −80 mV and +80 mV upon application of capsaicin (1 μM, red bar), DkTx (10 μM, orange bar), and ruthenium red (RR, gray bar) (n = 7). (*A*, *Right*) Current–voltage relationship traces (in 1-s^{-1} voltage-ramps between −80 mV to +80 mV) for the indicated points in *A*. (*B*) Mean/scatter-dot plot representing the amplitude of whole-cell currents in TREx HEK293T cells stably expressing rTRPV1 (V_m = +80 mV) at saturating DkTx concentration (10 μM, orange circles) and after subsequent 2 min of wash (green circles), normalized to the current amplitude of the saturating capsaicin response (1 μM) (n = 7); $^{**}P \leq 0.01$ (paired Student's t test). (*C*, *Left*) Representative current recording from an excised outside-out membrane patch of TREx HEK293T cells stably expressing rTRPV1 (V_m = +60 mV). Upward (outward) current indicates channel opening in response to capsaicin (1 μM,; red bar) or DkTx (1 μM, orange bar) application (n = 6). (*C*, *Right*) All-point amplitude histogram of capsaicin (i_{cap})- and DkTx (i_{DkTx})-evoked single-channel currents. The histogram was generated from the recording shown at the left. (*D*) Mean/scatter-dot plot is representing the amplitude of single-channel currents evoked by DkTx, applied at the indicated concentrations and capsaicin (1 μM) (n = 5–16). Statistical significance between the indicated DkTx concentrations and capsaicin are indicated as $^{***}P \leq 0.001$ (ANOVA followed by a multiple comparison test). (*E*) Mean/scatter-dot plot representing the Po of single-channel currents evoked by DkTx (1 μM, orange circles) and capsaicin (1 μM, red circles) (n = 6). Statistical significance is indicated as ns, not statistically significant (paired Student's t test). (*F*) Representative current recording from an excised outside-out membrane patch of TREx HEK293T cells stably expressing rTRPV1 upon application of capsaicin (1 μM, red bars), DkTx (1 μM, orange bar), and subsequent capsaicin application (V_m = +60 mV) (n = 4).

agonists were able to bind TRPV1 (*SI Appendix*, Fig. S2 *B* and *C*). Furthermore, capsaicin application to cells preexposed to DkTx evoked capsaicin-like current amplitude (*SI Appendix*, Fig. S2 *B* and *C*). Together, these results indicate that DkTx elicits lower current amplitude compared with capsaicin without modifying the capsaicin-evoked TRPV1 gating.

DkTx Evokes Low Unitary Conductance Currents in Comparison with Capsaicin. Distinct macroscopic current amplitudes evoked in an ion channel by its different activators could stem from differences in either open probability (Po) or current conductance. As

the slow dissociation rate of DkTx from TRPV1 warrants a persistent and stable activation of the channel (13, 21, 23), we set out to determine if the toxin evokes lower current amplitudes due to a diminished unitary conductance. To evaluate the single-channel properties evoked by DkTx, we analyzed the unitary conductance and Po of single TRPV1 channels in excised outside-out patches from HEK293T cells stably expressing rTRPV1. Membrane patches at a holding potential of +60 mV (to produce high current amplitude for the detection of changes in conductance) were initially perfused with a saturating capsaicin dose (1 μM). In patches containing a single channel, capsaicin was washed out followed by the addition of DkTx (Fig. 1*C*). Recordings were low-pass-filtered at 2 kHz. Single-channel current amplitudes were determined by generating all-point histograms and Gaussian distributions were fitted to the data (Fig. 1 *C* and *D*). As predicted, the Po of TRPV1 in response to DkTx was not statistically significant compared with that of the response to saturating capsaicin concentrations (Fig. 1*E*). However, as shown in Fig. 1 *C* and *D*, the DkTx-evoked currents had significantly lower amplitude (i_{DkTx} = 3.33 ± 0.20 pA; n = 6) compared with the capsaicin-evoked currents (i_{Cap} = 4.92 ± 0.14 pA; n = 6), denoting a reduction of 32.4 ± 5.6% in unitary conductance. It is noteworthy that all analyzed single-channel patches (n = 36), under various experimental conditions, displayed DkTx-evoked subconductance current (Fig. 1*D* and *SI Appendix*, Fig. S2*D*). These low-conductance currents elicited by DkTx were dose-independent, as applying different toxin concentrations did not alter the unitary conductance (Fig. 1*D*). As shown in *SI Appendix*, Fig. S2*D*, low unitary conductance in DkTx-activated TRPV1 was also observed in a holding potential of −60 mV, suggesting this evoked response is voltage-independent and of physiological relevance. This voltage independence likely underlies the low currents obtained in the whole-cell experiments throughout the voltage-ramp protocol (−80 to +80 mV; Fig. 1*A*). Also, consistent with the results obtained in whole-cell recordings (*SI Appendix*, Fig. S2 *B* and *C*), application of capsaicin to DkTx-activated single TRPV1 channels produced currents with a unitary conductance similar to those obtained when capsaicin was applied alone (Fig. 1*F*). To rule out that the observed differences in conductance reflect differences in gating transitions, we analyzed single-channel responses at different bandwidths (5 kHz and 2 kHz). This experimental setup demonstrated that the differences in conductance between TRPV1 activated by capsaicin and DkTx are independent of the filtering parameters (*SI Appendix*, Fig. S2*E*). Thus, we attribute the low current amplitude elicited by DkTx in whole-cell recordings to a subconductance state evoked by the toxin.

DkTx Binds rTRPV1 but Does Not Elicit Aversive Behavior in *C. elegans*. TRPV1's unique activation profile in response to DkTx raises the question of both the magnitude and duration of the resultant pain response in vivo. To assess the effect of DkTx on TRPV1-expressing sensory neurons, we expressed a rat TRPV1 transgene in *C. elegans*. Worms do not naturally express TRPV1, a trait which allows cell-specific transgenic expression of this sensory receptor (27). Indeed, previous studies from the Bargmann laboratory demonstrated that rTRPV1 could be functionally expressed in worms' polymodal nociceptive neurons (namely, ASH) to confer a specific, robust, and dose-dependent avoidance behavior to capsaicin (27, 28). We thus employed rTRPV1-transgenic worms to gain insight into DkTx-dependent TRPV1 activity in vivo (Fig. 2).

Behavioral tests were performed by placing drops containing the tested agonist in front of moving worms, and trials that elicited aversive-like responses were scored as positive withdrawal responses (Fig. 2*A*). As shown in Fig. 2*B*, DkTx elicits withdrawal responses in rTRPV1-transgenic, but not in WT, worms (N2). However, these DkTx-induced aversive responses were observed only in doses well above the in vitro saturating concentration of 1 μM toxin (≥12.5 μM; *SI Appendix*, Fig. S1*C*). The anterior ends

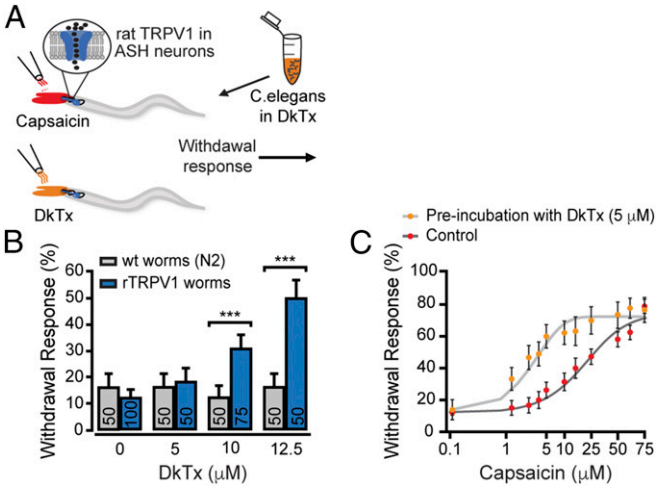

Fig. 2. DkTx sensitizes the aversive behavior evoked by capsaicin in rat TRPV1-transgenic worms. (*A*) Schematic representation of the withdrawal responses after addition of either capsaicin or DkTx drop in front of freely moving worms. (*B*) Withdrawal responses of WT (N2) and rTRPV1-expressing worms elicited by DkTx. Bars represent mean ± SEM, ***P < 0.001 (Mann–Whitney U rank tests were used for statistical analysis). (*C*) Capsaicin dose–response profiles for rTRPV1-expressing worms. Young adult worms were incubated for 15 min in bacteria-containing M13 buffer with or without DkTx (as described in *A*) prior to capsaicin challenge. Each point represents an average of ≥30 worms ± SEM. Lines are Boltzmann functions fit to the data.

of ASH neurons are exposed to the worm's exterior environment (29); hence, rTRPV1 channels expressed in ASH neurons are likely exposed to DkTx in our experimental settings. Moreover, because DkTx binds to an extracellular domain of the channel, its binding does not require crossing the plasma membrane.

Low concentrations of TRPV1 activators have been found to sensitize the channel toward other stimuli (30). To determine if applied DkTx is capable of binding rTRPV1 expressed in the worm's ASH neurons, we sought to analyze if it sensitizes the channel to capsaicin in subaversive concentrations. Indeed, preincubation of rTRPV1-transgenic worms with a nonaversive concentration of DkTx (5 μM) for 15 min before the behavioral assay significantly potentiated the withdrawal response evoked by capsaicin, as observed in the dose–response profiles (EC_{50} = 32.27 ± 6.19 vs. 3.76 ± 2.73 μM control and preincubated with DkTx, respectively; Fig. 2*C*). This potentiation indicates that DkTx binds to rTRPV1 in transgenic *C. elegans* ASH neurons in concentrations that do not evoke withdrawal responses. Thus, our results suggest that while DkTx binds to rTRPV1 it fails to elicit subsequent behavioral responses.

The Monomeric Knots K1 and K2 Elicit Higher Conductance than the Bivalent DkTx. To elucidate the molecular determinants of the DkTx-induced subconductance, we analyzed the role of the different toxin components in TRPV1 activation. The two ICK motifs that comprise DkTx (i.e., K1 and K2) are highly homologous yet differ in their potency, affinity, and binding orientation to the TRPV1 channel (13, 21). Furthermore, in contrast to the irreversibility of the full-length toxin, the separated single knots were shown to act as reversible TRPV1 activators (13, 21, 25). Thus, we sought to determine whether these two single knots could elicit currents with unitary conductance different from that evoked by DkTx. Single TRPV1 channel recordings showed that when applied as monomers both knots evoked reversible currents with higher unitary conductance compared with WT DkTx (Fig. 3*A*). It is noteworthy that the increase in unitary conductance was more pronounced in K2-evoked currents, resembling that of capsaicin (88.8 ± 1.3%). Moreover, whole-cell recordings of K1- and K2-evoked responses

PHARMACOLOGY

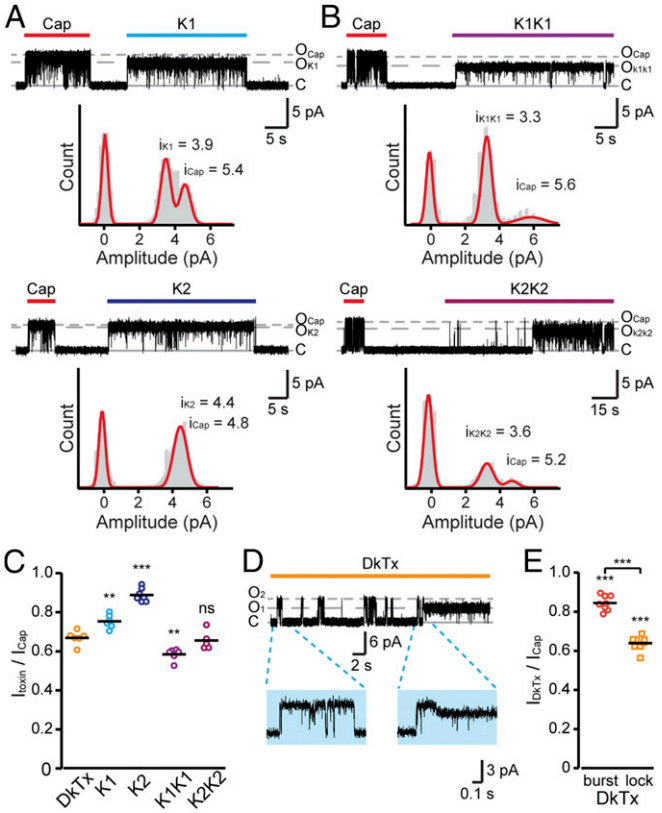

Fig. 3. The single knots constituting DkTx evoke higher unitary conductance currents in comparison with the bivalent toxins. (*A*, *Top*) Representative current recordings from an excised outside-out membrane patch of TREx HEK293T cells stably expressing rTRPV1 (treated as described in Fig. 1). Representative recordings are shown after exposing the patch to capsaicin (1 μM, red bar) and K1 (100 μM, cyan bar) (V_m = +60 mV) (n = 6). Trace is accompanied by an all-point amplitude histogram generated from the recording shown above. (*A*, *Bottom*) Representative current recordings from an excised outside-out membrane patch of TREx HEK293T cells stably expressing rTRPV1 (treated as described in Fig. 1). Representative recordings are shown after exposing the patch to capsaicin (1 μM; red bar) and K2 (50 μM; dark blue bar) (V_m = +60 mV) (n = 7). Trace is accompanied by an all-point amplitude histogram generated from the recording shown above. (*B*, *Top*) Representative current recordings from an excised outside-out membrane patch of TREx HEK293T cells stably expressing rTRPV1 (treated as described in Fig. 1). Representative recordings are shown after exposing the patch to capsaicin (1 μM, red bar) and K1K1 (15 μM, purple bar) (V_m = +60 mV) (n = 6). Trace is accompanied by an all-point amplitude histogram generated from the recording shown above. (*B*, *Bottom*) Representative current recordings from an excised outside-out membrane patch of TREx HEK293T cells stably expressing rTRPV1 (treated as described in Fig. 1). Representative recordings are shown after exposing the patch to capsaicin (1 μM, red bar) and K2K2 (15 μM, magenta bar) (V_m = +60 mV) (n = 5). Trace is accompanied by an all-point amplitude histogram generated from the recording shown above. (*C*) Mean/scatter-dot plot representing the ratio between amplitudes of the single-channel current evoked by the indicated toxin and capsaicin at +60 mV (n = 5–8). Mutated toxins were compared with DkTx as well as with each other for statistical analysis. ns, not statistically significant; $^{**}P \leq 0.01$; $^{***}P \leq 0.001$ (ANOVA followed by multiple comparison test). (*D*) Representative current recordings from an excised outside-out membrane patch of cells expressing rTRPV1. Upward (outward) current indicates channel opening (gray dashed lines) in response to DkTx (1 μM, orange bar) application. Holding potential was at +60 mV. Blue background insets show higher magnification of indicated 1 s of DkTx-evoked response. (*E*) Mean/scatter-dot plot representing the ratio between the single-channel current amplitude of DkTx-induced initial bursts ("burst", red circles) or continuous ("lock", orange squares) activations and capsaicin (n = 9). Statistical significance between normalized DkTx-evoked responses and capsaicin are indicated as $^{***}P \leq 0.001$ (ANOVA followed by multiple comparison test).

in rTRPV1-expressing HEK293T cells showed higher macroscopic current amplitudes compared with the DkTx-evoked response (*SI Appendix*, Fig. S3). Importantly, the K2-evoked response was significantly stronger than that evoked by K1 (79.1 ± 1.4% and 71.1 ± 1.3% of capsaicin-evoked response, respectively), indicating a correlation between unitary conductance and macroscopic current amplitudes (*SI Appendix*, Fig. S3).

As both monomeric knots failed to recapitulate the low unitary conductance currents elicited by the full-length DkTx, we sought to determine the role of the toxin's linker in producing DkTx's unique TRPV1 activation profile. If the linker imposes moderate conductance, homologous ICK motifs' bivalent toxins (i.e., K1K1 and K2K2) containing DkTx linker will evoke a subconductance state, similar to DkTx. Indeed, as shown in Fig. 3*B*, both homobivalent toxins elicited currents with unitary conductance similar to the native heterobivalent DkTx (normalized to capsaicin: DkTx; 67.7 ± 4.1%, K1K1; 58.5 ± 1.2%, K2K2; 63.5 ± 1.1%). The difference in unitary conductance evoked by homobivalent toxins and the single-knot toxins (Fig. 3*C* and *SI Appendix*, Table S1) suggests that the toxin's linker restricts TRPV1 conductance upon DkTx binding.

The affinity of K2 to TRPV1 is higher than that of K1 (13, 21). It was predicted that during binding of DkTx, K2 binds to the channel first and mediates subsequent binding of the less-potent K1 to produce a bivalent interaction between the toxin and TRPV1 (21). Hence, it is conceivable that binding of DkTx to TRPV1 transiently elicits an increased unitary conductance current representing K2-evoked response and that this conductance is lowered upon K1 binding or returns to baseline if detachment of K2 occurs. Indeed, we observed a number of short activity bursts during DkTx application in several recordings, before the channel was locked in a stable open state (Fig. 3*D*). These short bursts of channel activity were mainly observed at subsaturating toxin concentration (0.5 μM). Of note, these activation bursts displayed high unitary conductance which was similar to that evoked by capsaicin (84.8 ± 2.1%), potentially reflecting the initial binding of K2 to TRPV1 (Fig. 3*E*). Together, our results demonstrate that each of the toxin knots evokes higher unitary conductance currents that were significantly different from the bivalent toxins.

Elongating the DkTx Linker Shifts the Evoked TRPV1 Unitary Conductance. DkTx's two ICKs bind two neighboring subunits in the outer pore domain of the tetrameric TRPV1 channel (23, 31). The toxin's linker, which connects these ICKs, is composed of 7 aa including two proline residues that reduce its flexibility (21). Thus, we hypothesized that the linker alters TRPV1 activation and elicits subconductance states. To test this hypothesis, we engineered a toxin with a longer linker [DkTx(DL)], by introducing seven additional glycine residues. Whole-cell recordings showed that the DkTx(DL)-evoked current is persistent, similar to WT DkTx. However, the current amplitude elicited by this engineered toxin was comparable to that evoked by the single monomeric knots (K1 and K2) (Fig. 4 *A*–*C*; cf. *SI Appendix*, Fig. S3). In addition, application of DkTx(DL) to outside-out patches containing a single TRPV1 channel resulted in high subconductance currents which were similar to those elicited by the single knot K1 (76.8 ± 2.9% of capsaicin response; Fig. 4 *D* and *E*, compared with Fig. 3 *A* and *C* and *SI Appendix*, Table S1). Thus, our results demonstrate that the length and flexibility of the toxin's linker are involved in determining the current amplitude of DkTx-induced TRPV1 currents.

Concentration–response relationships produced by live-cell calcium imaging indicated that DkTx(DL) has lower potency than WT DkTx [DkTx: EC_{50} = 0.11 ± 0.01 μM, n_H = 1.5 ± 0.1; DkTx(DL): EC_{50} = 0.54 ± 0.08 μM, n_H = 1.4 ± 0.2]. It is noteworthy that, similar to DkTx, the DkTx(DL) is more potent than each of the single knots (13, 21). In addition, DkTx(DL) is more efficacious than DkTx at relative saturating concentrations [$DkTx_{(1.5\ \mu M)}$: $F_{Toxin}/F_{Capsaicin}$ = 0.86 ± 0.02, $DkTx(DL)_{(3.5\ \mu M)}$: $F_{Toxin}/F_{Capsaicin}$ = 0.94 ± 0.01; *SI*

Appendix, Fig. S4]. The strong responses and the similar efficacy of the two toxins obtained in live-cell calcium imaging experiments could be attributed to the limited dynamic range of the Ca^{2+}-sensitive dye (compared with the whole-cell recordings; Fig. 4 *A*–*C*) (32).

To assess whether elongating the linker alters the toxin-evoked aversive response in vivo, we challenged rTRPV1-transgenic worms with DkTx(DL) (as described for the WT DkTx; Fig. 2). As shown in Fig. 4*F*, DkTx(DL) produced stronger withdrawal responses in transgenic worms in comparison with DkTx at concentrations ≥10 μM. Overall, these results indicate that lengthening the DkTx linker evokes a stronger behavioral response due to the increase in TRPV1 current's magnitude.

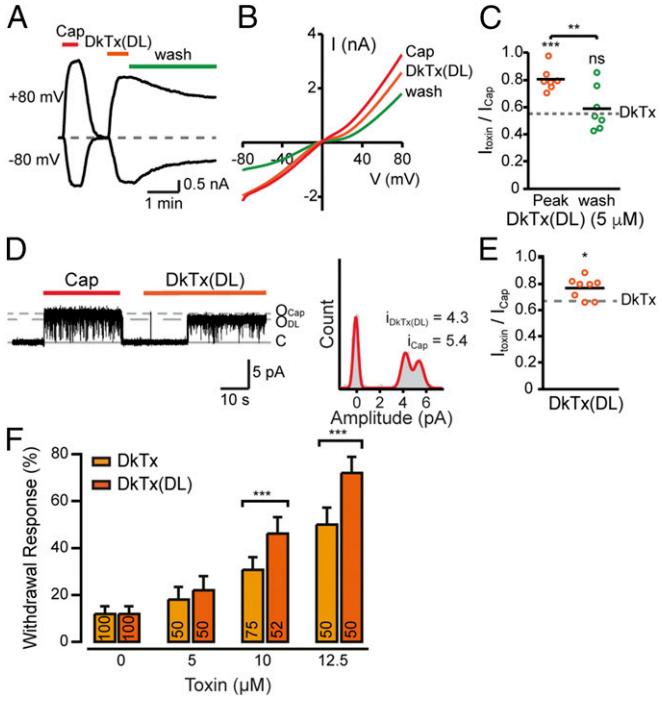

Fig. 4. Elongating the toxin's linker increases the evoked current amplitude. (*A*) Representative whole-cell current trace from TREx HEK293T cells stably expressing rTRPV1 at −80 mV and +80 mV upon application of capsaicin (1 μM, red bar) and DkTx(DL) (5 μM, orange bar) ($n = 7$). (*B*) Current–voltage relationship traces in TREx HEK293T cells stably expressing rTRPV1 in response to capsaicin (Cap, 1 μM, red line), DkTx(DL) (5 μM, dark orange line), and DkTx (DL) washout (Wash, 2 min) ($n = 7$). (*C*) Mean/scatter-dot plot representing the amplitude of whole-cell currents in TREx HEK293T cells stably expressing rTRPV1 ($V_m = +80$ mV) at a saturating DkTx(DL) concentration (5 μM, peak, orange circles) and after subsequent 2 min of wash (wash, green circles), normalized to the current amplitude of the saturating capsaicin response (1 μM) ($n = 7$). The dashed line indicates the average ratio of DkTx- and capsaicin-evoked peak amplitudes at +80 mV. Statistical significance between normalized responses of DkTx(DL) at peak and wash and DkTx are indicated as ns, not statistically significant, $^{**}P \leq 0.01$ and $^{***}P \leq 0.001$ (ANOVA followed by a multiple comparison test). (*D*, *Left*) Representative current recordings from an excised outside-out membrane patch of TREx HEK293T cells stably expressing rTRPV1 (treated as described in Fig. 1). Representative recordings are shown after exposing the patches to capsaicin (1 μM, red bar) and DkTx(DL) (5 μM, dark orange bar) ($V_m = +60$ mV) ($n = 8$). (*D*, *Right*) All-point amplitude histogram generated from the recording shown on the left. (*E*) Mean/scatter-dot plot representing the ratio between amplitudes of the single-channel current activated by DkTx(DL) and capsaicin at +60 mV ($n = 8$). The dashed line indicates the average ratio of DkTx- and capsaicin-evoked current amplitudes at +60 mV. Statistical significance between normalized responses of DkTx(DL) and DkTx are indicated as $^{*}P \leq 0.05$ (unpaired Student's *t* test). (*F*) Withdrawal responses of rTRPV1-expressing worms elicited by DkTx and DkTx(DL). Bars represent mean ± SEM, $^{***}P \leq 0.001$ (Mann–Whitney *U* rank tests were used for statistical analysis).

Deletion of the TRPV1 Pore Turret Results in Maximal DkTx-Evoked Current Conductance. While our results indicate that DkTx induces a subconducting opening of the TRPV1 pore, the TRPV1–DkTx/RTX structure obtained by cryo-EM was suggested to represent a fully open state of the channel (23). However, a minimal construct of TRPV1, devoid of the pore turret and portions of N and C terminals, was used for the cryo-EM structural analysis to improve the channel's chemical stability (illustrated in Fig. 5*A*) (31). Thus, we sought to determine whether these TRPV1 structural features influence the DkTx-evoked current. To this end, we analyzed the response of this minimal ("cryo") channel to this toxin. In contrast to the WT TRPV1, whole-cell recordings of cells expressing cryo TRPV1 showed that DkTx produces higher current amplitudes than those evoked by capsaicin (Fig. 5 *B* and *D*; cf. Fig. 1 *A* and *B*) (31). Indeed, capsaicin was previously reported to act as a partial agonist in this construct (26). While the intracellular N and C terminals are unlikely to affect DkTx-induced channel activation, the pore turret resides within the TRPV1 outer pore region (between S5 and the pore helix), next to the DkTx binding site (21). Thus, to characterize the effect of this specific domain, we constructed a TRPV1 channel lacking the pore turret (TRPV1Δ23; Fig. 5*A*). Similar to cryo TRPV1, TRPV1Δ23's response to DkTx was stronger than its response to capsaicin (TRPV1: $I_{DkTx\ 2\ \mu M}/I_{Capsaicin} = 54.5 \pm 2.3\%$; TRPV1Δ23: $I_{DkTx\ 2\ \mu M}/I_{Capsaicin} = 217.7 \pm 16\%$; Fig. 5 *C* and *D*).

To evaluate the properties of DkTx- and capsaicin-mediated activation of these mutated channels, single-channel currents were recorded. In both cryo TRPV1 and TRPV1Δ23 channels, DkTx evoked maximal unitary conductance currents similar to capsaicin. Thus, deletion of the pore turret enabled DkTx to elicit a full opening of the TRPV1 channel (Fig. 5 *E* and *F*). Interestingly, the dwell time of capsaicin-induced currents in TRPV1Δ23 channels was dramatically reduced compared with WT TRPV1 (TRPV1: 114.6 ± 41.1 ms; Δ23 TRPV1: 1.1 ± 0.2 ms; Fig. 5 *E* and *G* compared with Fig. 1*C*). Thus, this result is in accordance with the data obtained in whole-cell recordings where DkTx elicited a stronger activation of TRPV1Δ23 than capsaicin did. Noteworthy, the dwell time of the DkTx-evoked current in TRPV1Δ23 is also reduced compared with the DkTx-evoked current in WT (TRPV1: 465.1 ± 96.3 ms; TRPV1Δ23: 195.6 ± 77.5 ms; Fig. 5 *E* and *G* compared with Fig. 1*C*). Interestingly, TRPV1Δ23 was less sensitive to capsaicin as saturating responses in whole-cell recordings were achieved at 10 μM capsaicin, compared with 1 μM in WT rTRPV1 (*SI Appendix*, Fig. S5*A*). Nonetheless, the response of TRPV1Δ23 to saturating capsaicin concentrations was still significantly lower than its response to DkTx (*SI Appendix*, Fig. S5*A*). Additionally, we observed a capsaicin-evoked low Po of channel activation in outside-out patches containing TRPV1Δ23 at both 10 and 30 μM concentrations (*SI Appendix*, Fig. S5*B*).

To define whether deletion of the turret resulted in different DkTx binding properties, we determined the dose–response of DkTx-mediated activation of TRPV1Δ23 using live-cell calcium imaging. Concentration–response curves were generated in WT and TRPV1Δ23 by normalizing the peak of the calcium response for the analyzed toxin concentration to the maximal response to DkTx in the same construct. As shown in *SI Appendix*, Fig. S5*C*, DkTx potency is comparable in WT and TRPV1Δ23 (TRPV1: $EC_{50} = 90 \pm 5$ nM, $n_H = 2 \pm 0.2$; TRPV1Δ23: $EC_{50} = 60 \pm 4$ nM, $n_H = 1.5 \pm 0.1$). To examine whether the deletion of the turret affects the channel response to other modalities, we evaluated the response of the TRPV1Δ23 channel to protons. The ratio of the whole-cell current amplitude evoked by pH 5.5 and capsaicin was preserved between WT and TRPV1Δ23, suggesting that, similar to capsaicin-induced gating, deletion of the pore turret affected the proton-evoked response (*SI Appendix*, Fig. S6 *A* and *B*). Previous studies have shown that the pore turret is involved

PHARMACOLOGY

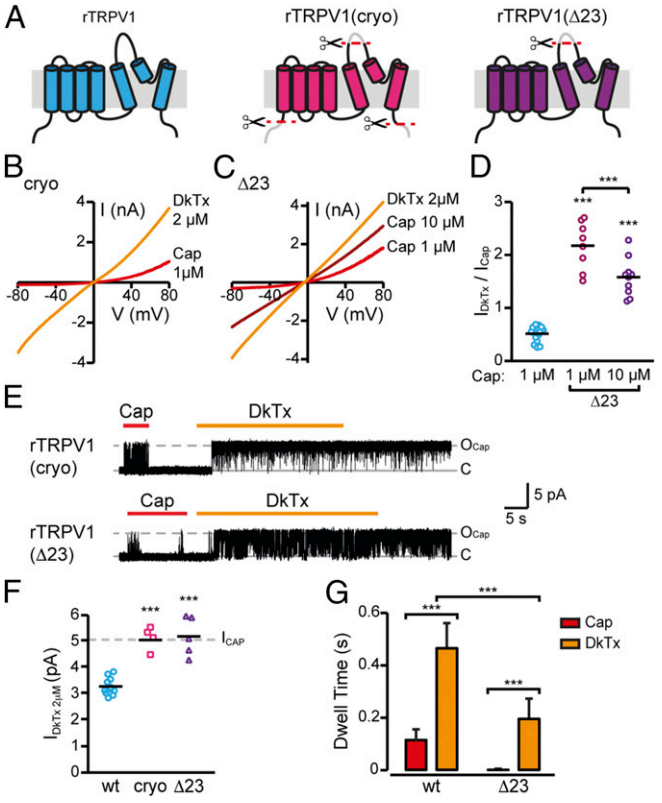

Fig. 5. DkTx evokes full conductance in TRPV1 channels lacking the pore turret. (*A*) Schematic illustrations depicting the location of deleted regions in the different TRPV1 constructs. (*B*) Current–voltage relationship traces in TREx HEK293T cells expressing cryo rTRPV1 in response to 1 μM capsaicin (Cap 1 μM, red line) and DkTx (2 μM, orange line) ($n = 5$). (*C*) Current–voltage relationship traces in TREx HEK293T cells expressing rTRPV1Δ23 in response to 1 μM capsaicin (Cap 1 μM, red line), 10 μM capsaicin (Cap 10 μM, dark red line), and DkTx (2 μM, orange line) ($n = 8$). (*D*) Mean/scatter-dot plot representing the ratio between amplitudes of the whole-cell current activated by DkTx (2 μM) and the indicated capsaicin concentration at +80 mV ($n = 8$–16). Capsaicin responses in TRPV1Δ23 were compared with the capsaicin response in WT TRPV1 as well as with each other for statistical analysis. ***$P \leq 0.001$ (ANOVA followed by multiple comparison test). (*E*, *Top*) Representative current recordings from an excised outside-out membrane patch of TREx HEK293T cells expressing cryo rTRPV1 (treated as described in Fig. 1). Representative recordings are shown after exposing the patches to capsaicin (1 μM, red bar) and DkTx (2 μM, orange bar) ($V_m = +60$ mV) ($n = 4$). (*E*, *Bottom*) Representative current recordings from an excised outside-out membrane patch of TREx HEK293T cells expressing TRPV1Δ23 (treated as described in Fig. 1). Representative recordings are shown after exposing the patches to capsaicin (1 μM, red bar) and DkTx (2 μM, orange bar) ($V_m = +60$ mV) ($n = 5$). (*F*) Mean/scatter-dot plot representing the amplitude of single-channel currents evoked by 2 μM DkTx in TRPV1 (cyan circles), cryo TRPV1 (pink squares), and TRPV1Δ23 (purple triangles) at +60 mV ($n = 4$–11). Statistical significance between the indicated mutant TRPV1 channels and WT TRPV1 is indicated as ***$P \leq 0.001$ (ANOVA followed by a multiple comparison test). (*G*) Dwell time of TRPV1 single-channel current elicited by capsaicin (1 μM, red bars) and DkTx (2 μM, orange bars) ($n = 6$–8). Bars represent mean ± SEM, ***$P \leq 0.001$ (ANOVA followed by multiple comparison test).

in TRPV1 activation by temperature; thus, we tested the TRPV1Δ23 response to heat by live-cell Ca^{2+} imaging (33, 34). Our results show that the ratio between rTRPV1Δ23 responses to DkTx and heat (44 °C) is increased twofold compared with the ratio measured for the WT receptor (*SI Appendix*, Fig. S6*C*). Together, these results indicate that deletion of the TRPV1 pore turret differently affects the activation profile by the channel's different agonists. Our results indicate that while the TRPV1 turret region mediates the low unitary conductance evoked by DkTx, this structural element also acts to stabilize the open channel state in response to other modalities, such as capsaicin, protons, and heat.

DkTx Produces a Robust Aversive Response in *C. elegans* Expressing TRPV1Δ23. To test whether the full conductance response evoked by DkTx in TRPV1Δ23 resulted in a stronger aversive behavior in vivo, we challenged worms expressing either WT TRPV1 or TRPV1Δ23 with DkTx. As shown in Fig. 6*A*, TRPV1Δ23-transgenic worms were more sensitive to the toxin than WT TRPV1-transgenic worms. Notably, at 5 μM toxin concentration, DkTx evoked a robust aversive behavior in TRPV1Δ23-transgenic worms (~50% of the tested worms), while the DkTx-evoked response was similar to the baseline response in worms expressing the WT channel (~20% of the tested worms). This enhanced aversive behavior to DkTx appears to be at the expense of the response to capsaicin, as TRPV1Δ23-transgenic worms were less sensitive to this agonist than WT TRPV1-transgenic worms, albeit this difference was significant at higher capsaicin concentrations (Fig. 6*B*). Altogether, our results (electrophysiology and behavior) suggest that TRPV1 channels lacking the pore turret bind DkTx more effectively and conduct larger currents than the WT channels, while the response to capsaicin is impaired.

The TRPV1 Pore Turret Is Flexible and Crowds the Extracellular Vestibule. Given the length of the pore turret, its proximity to the DkTx binding site, and its dramatic effect on the toxin-induced current, we speculated that this element might interfere with ion flow across the TRPV1 pore, particularly upon activation by WT DkTx; consistently, turret deletion would lead to maximal currents. To examine whether this effect might entail a well-defined conformation of the turret, we substituted three proline residues in the rTRPV1 sequence by alanine (P608A, P613A, P623A; TRPV1_3P-A), reasoning that these prolines might confer structural rigidity to this element. However, the DkTx-induced activation profile was comparable in TRPV1_3P-A and WT TRPV1 (*SI Appendix*, Fig. S7). We also examined whether specific interactions formed by the turret (with the toxin, for example) might explain its functional effect, by replacing all pore turret residues by either glycine or serine (TRPV1_GS). Strikingly, however, the response of this construct to DkTx activation was similar to that of WT TRPV1 (*SI Appendix*, Fig. S7). These observations demonstrate that neither the identity of the residues in the pore turret nor its precise 3D structure explain the influence of this element on DkTx-induced channel activation. Instead, these data indicate that the pore

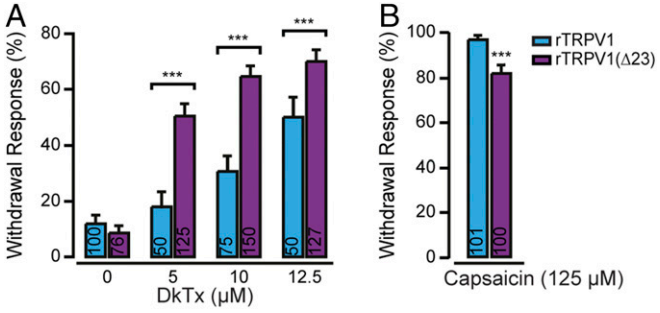

Fig. 6. DkTx produces a robust activation of TRPV1 lacking the pore turret. (*A*) DkTx-induced withdrawal responses of worms expressing rTRPV1 or TRPV1Δ23. Bars represent mean ± SEM, ***$P \leq 0.001$ (Mann–Whitney *U* rank tests were used for statistical analysis). (*B*) Capsaicin-induced withdrawal response of worms expressing rTRPV1 or TRPV1Δ23. Bars represent mean ± SEM, ***$P \leq 0.001$ (Mann–Whitney *U* rank tests were used for statistical analysis).

turret is a flexible, dynamic structural element that sterically hinders the extracellular side of the TRPV1 pore, resulting in subconductance currents.

To substantiate or refute this hypothesis, we resorted to molecular modeling. Specifically, we used the knowledge-based, structure-prediction algorithm ROSETTA (35) to construct models of the four pore turrets missing in the cryo-EM structure of rTRPV1. The first set of models was constructed for the channel bound to WT DkTx (Fig. 7*A*). Consistent with the notion that the turret is dynamic, ROSETTA produced a highly diverse set of turret conformations, for all four channel subunits (Fig. 7*B*). These ensembles, however, are not identical. For the two subunits where the turret truncation site is directly underneath DkTx, the ensemble is split into two subsets, each at either side of the toxin linker (Fig. 7*B*). It could be argued, however, that the set of turret conformations found more peripherally than the linker ought to be discounted. The reason is that DkTx naturally resides in the lipid bilayer, implying that it docks onto TRPV1 laterally, from the periphery of the channel (21). Thus, binding of DkTx will very likely enclose and limit the ensemble of turret conformations, for two of the channel subunits; to illustrate this concept, we show a second set of models developed under this premise in Fig. 7*C*. Regardless of this consideration, however, analysis of the pore dimensions for each of the ROSETTA models shows that, on average, the presence of the turret drastically reduces the volume of the outer vestibule of the permeation pore, compared with the DkTx-bound TRPV1 cryo-EM construct (Fig. 7*D*). This effect is more pronounced for the case in which the DkTx linker encloses the ensemble of turret conformations, which, as mentioned, we believe to be more realistic. Conversely, either the absence of the linker or its elongation ought to reverse this crowding effect, to some degree. Indeed, analysis of the pore dimensions for a third set of turret models (Fig. 7 *E* and *F*) shows that, on average, the outer vestibule is wider than that in the TRPV1/DkTx complex, though it is still substantially narrower than the pore in TRPV1 cryo/DkTx (Fig. 7*G*). In summary, these data explain why DkTx-activated TRPV1 current magnitudes are greater for the TRPV1 cryo-EM construct than for the WT channel. It also appears to be consistent with the observation that, for WT TRPV1, elongation or deletion of the toxin linker results in larger currents than those evoked by intact DkTx.

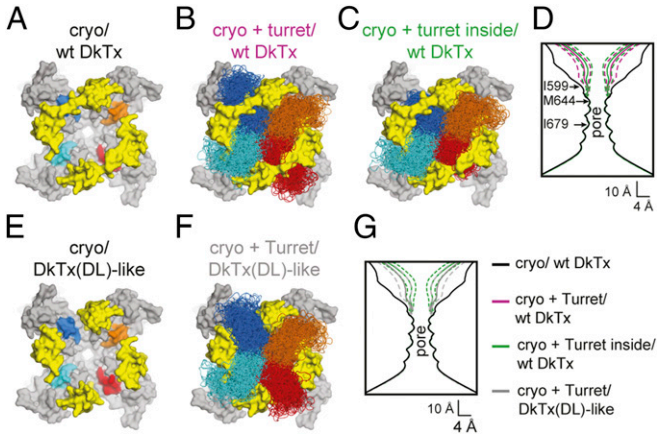

Fig. 7. Molecular modeling suggests TRPV1 pore turret hinders ion conduction. (*A*) Cryo-EM structure of cryo rTRPV1 (gray surface) with DkTx bound (yellow surface), viewed along the pore from the extracellular side (24). The locations of the pore-turret truncation are indicated in colors (blue, cyan, red, and orange). (*B*) Models of rTRPV1 including the pore turret, produced with ROSETTA. Shown are 200 pore-turret conformations for each channel subunit, colored as in *A*. (*C*) Same as in *A*, using an alternative scoring protocol that favors models whereby the pore turrets added to the two-channel subunits underneath DkTx (blue and red) are enclosed by the toxin linkers, on account of the likely fact that DkTx docks onto TRPV1 laterally, from the membrane. (*D*) Calculated pore-diameter profile for the cryo-EM structure of rTRPV1 cryo/wt DkTx (black), compared with averages calculated for the ensemble of models shown in *B* and *C* (magenta and green, respectively). Solid lines represent the average profiles; dashed lines indicate the dispersion (SD) of each sample. (*E*) Same as *A*, after deletion of the toxin linkers [DkTx(DL)-like]. (*F*) Same as *B*, based on the assumed structure of the complex shown in *E*. (*G*) Same as *D*, now comparing rTRPV1 models (with the pore turrets) in complex with WT DkTx (green) or with DkTx lacking the linker (gray), and the cryo-EM structure of rTRPV1 cryo/wt DkTx (black).

Discussion

TRPV1 is a multisteric receptor that can be activated by a variety of ligands to produce different activation patterns leading to distinct neuronal responses (11, 30, 36, 37). Here, we investigated the activation mechanism of TRPV1 by the bivalent tarantula toxin DkTx and the phytotoxin capsaicin. Our results indicate that in cells expressing TRPV1, DkTx evokes a lower current amplitude compared with capsaicin, similar to the activation profile reported in reconstituted proteoliposomes and trigeminal neurons (7, 13). Thus, this apparent DkTx-mediated subdued TRPV1 activation is an intrinsic property of the channel and occurs in its native environment. Using single-channel recordings, we showed that the moderate DkTx-evoked TRPV1 activation stems from a lower unitary conductance of the produced current compared with capsaicin. Furthermore, data obtained in transgenic worms expressing rTRPV1 in a couple of sensory neurons demonstrated that subaversive DkTx concentrations were capable of amplifying the capsaicin-evoked withdrawal responses, indicating that while the toxin binds to the receptor it elicits only subthreshold neuronal depolarization. To elucidate the molecular mechanism underlying the toxin's unique ability to evoke irreversible subconductance activation of TRPV1, we engineered several DkTx and TRPV1 constructs. We found that elongating the toxin's linker resulted in a higher subconductance of TRPV1 currents. Importantly, deletion of the channel pore turret resulted in full-channel conductance in response to DkTx, which was comparable to that evoked by capsaicin. Furthermore, deletion of the turret region led to a robust DkTx-evoked withdrawal response in transgenic worms. Together, our results demonstrate that DkTx elicits a distinct TRPV1 gating modality, which is governed by the channel pore turret and leads to distinct responses at both the molecular and behavioral levels (Figs. 6 and 7).

Recently, the TRPV1 structure in its DkTx-bound state was solved at near-atomic resolution using cryo-EM and molecular dynamics (21, 24). This channel structure at its putative fully open state revealed that the two ICK motifs of DkTx bind adjacent TRPV1 subunits, while the linker connecting them adopts a tensed conformation (24). However, the TRPV1 channel construct used for the structure determination lacks the sizeable pore turret in the outer pore region, and therefore the structural basis for the functional impact of this truncation is far from evident. As a first approximation, however, it is reasonable to posit that the channel conductance might depend on the presence or absence of the turret because this element would hinder ion flow across the extracellular vestibule of the permeation pore. Indeed, in structural models of TRPV1 including the four pore turrets, this region becomes much narrower than in the truncated channel, effectively extending the most confined portion of the pore for almost 20 Å. This effect is particularly significant when the channel is bound to DkTx, as the toxin linker fosters conformations of the pore turret that crowd the center of the pore. Accordingly, our results show larger channel conductance when the toxin's linker is elongated, or when the pore turrets are omitted, which we interpret as evidence that the steric hindrance

imposed by these elements is alleviated or eliminated. Additional effects not specifically considered in our structural modeling analysis cannot be discounted. Truncation of the pore turrets might alter the configuration and dynamics of the selectivity filter or one or more of the mechanisms of activation of the channel. Indeed, it was shown that the outer pore region of TRPV1 plays a critical role in channel gating (13, 24, 26, 38–41). This domain was further found to be involved in channel inhibition by several animal toxins and monovalent cations (26, 42, 43). Accordingly, perturbations to the structure of the outer pore region were reported to contribute to the low TRPV1 unitary conductance elicited by protons (44). Furthermore, oxytocin was found to activate TRPV1 through a binding site which is at least partially convergent with the DkTx binding site (45). While the unitary conductance evoked by oxytocin was found to be 81 pS, similar to K2 and capsaicin, these measurements were conducted at different settings (e.g., planar lipid bilayer) (45). Specifically, the pore turret was suggested to be involved in conformational rearrangements during heat activation of TRPV1 (33, 34). Nonetheless, the turret-deleted TRPV1 construct retains sensitivity, although altered, to heat (*SI Appendix*, Fig. S6*C*) (26). While both DkTx and heat evoke conformational changes in the outer pore region and the turret, heat does not potentiate the response to DkTx and DkTx does not lower the heat activation threshold (26). TRPV1 response to other modalities also involves the channel's turret. It was shown that mutating the pore turret reduced TRPV1 activation by the centipede toxin RhTx (14). Also, FRET measurements revealed that Mg^{2+} ions produce conformational changes in the pore turret and evoke subconductance activation of TRPV1 (40). However, the reduced conductance could be attributed to the relatively low permeability of Mg^{2+} through TRPV1 (40). The pore helix is a direct extension of the pore turret (46). It was shown, in both cryo-EM analysis and molecular dynamics simulations, that the motion of the pore helix regulates the pore radius at the selectivity filter (24, 47). Thus, perturbing the movement of the pore turret by DkTx may affect the position of the pore helix and consequently the conductance through the selectivity filter. As the TRPV1–DkTx cryo-EM structure also includes RTX bound to the channel's vanilloid binding site (23, 24), solving the full TRPV1 structure when it is solely bound to DkTx is required to shed more light on the gating mechanism induced by this toxin.

In accordance with previous findings by Jara-Oseguera et al. (26), our data further demonstrate that capsaicin acts as a partial TRPV1 agonist upon deletion of the channel turret, as it produces significantly lower macroscopic currents amplitude in comparison with DkTx. Interestingly, we found that the diminished response to capsaicin stems from the reduced mean open time of TRPV1Δ23 compared with the native receptor. This observation may explain why in the cryo-EM structure the channel appears to be captured with an open lower gate and a closed selectivity filter when bound to capsaicin (23). It is, therefore, possible that the pore turret stabilizes the opening of TRPV1 selectivity filter when activated by capsaicin via allosteric modulation.

While the knots that comprise DkTx, K1 and K2, share binding sites on TRPV1, they adopt a different orientation when bound to this receptor, reflecting the structural differences between the two lobes (21). These differences also underlie dissimilarities in their TRPV1 activation properties (i.e., the higher potency of K2 compared with K1) (13, 21, 25). In this study, we show that as a monomer K2 evokes full activation of TRPV1, which was comparable to that of capsaicin (Fig. 3 *A* and *C*). In contrast, application of monomeric K1 resulted in a slightly, but significantly, reduced conductance, thus confirming it as a weaker TRPV1 activator (Fig. 3 *A* and *C*). Furthermore, these results imply that in addition to the toxin's linker, the K1 knot may play a role in the observed low TRPV1 conductance. Single-channel currents evoked by the homobivalent toxins, K1K1 and K2K2, were characterized by low unitary conductance currents similar to those obtained by DkTx (Fig. 3 *B* and *C* and *SI Appendix*, Table S1). This finding suggests that the DkTx-evoked subdued TRPV1 activation and reduced conductance do not stem from the asymmetric binding of K1 and K2 but instead are directed by the toxin's bivalency. However, the similar unitary conductance evoked by DkTx(DL) and monomeric K1 suggests that this knot may also limit TRPV1 activation (compare Figs. 3 and 4 and *SI Appendix*, Table S1). Interestingly, we observed that DkTx could evoke several bursts of activity with high conductance, which were quickly followed by a stable, persistent, low conductance current (Fig. 3 *D* and *E*). Because the native toxin's linker reduces TRPV1 conductance, it is possible that this observation represents an initial binding of one of the ICK motifs (likely K2) and a subsequent binding of its counterpart (i.e., K1), which restricts the movement at the outer pore region.

Our results further suggest that DkTx potentiates TRPV1 activation by other activators (Fig. 2*C*). In recent years, several TRPV1-modulating animal toxins were characterized (14, 46, 48). These peptide toxins, including DkTx, were found to bind to the outer pore region of the channel (14, 15, 46, 48). One of these toxins, RhTx, was shown to enhance heat-dependent activation of TRPV1 in nanomolar concentrations (14). Thus, it is possible that at physiologically relevant concentrations peptide toxins targeting TRPV1 outer pore region act to potentiate the channel response to common endogenous activators such as heat, protons, and/or inflammatory mediators.

Materials and Methods

Recombinant Toxin Generation. pLic-MBP-toxin plasmids encode a fusion protein which includes the toxin, a MalE signal sequence for periplasmic export, a His_6 affinity tag for protein purification, maltose-binding protein (MBP), which enhances solubility, and a tobacco etch virus (TEV) recognition site preceding the toxin (49). pLic-MBP-toxin plasmids were transformed into BL21(DE3) bacteria (New England Biolabs). Transformed bacteria were grown at 37 °C in Luria Bertani medium supplemented with 100 μg/mL ampicillin (Gold Biotechnology) at 180 rpm. At OD_{600} = 0.8–1.0 cultures were cooled down to 16 °C and fusion protein expression was induced with 250 μM isopropyl-β-D-thiogalactopyranoside (Inalco) at 180 rpm. Fourteen hours later cells were harvested by centrifugation at 6,000 × *g* and 4 °C for 15 min. Cell pellet was resuspended in buffer A (NaCl 500 mM, sodium phosphate 40 mM, imidazole 20 mM, $MgCl_2$ 2 mM, DNaseI 10 μg/mL, and PMSF 1 mM, pH 8.0) and was then passed through a precooled homogenizer. The homogenized cells were then lysed by using a cell disruptor (M-110S Microfluidizer Processor; Microfluidics) at 80 kPa. The lysate was collected and centrifuged at 50,000 × *g* and 4 °C for 30 min. The His_6-MBP-toxin fusion protein was then captured by passing the supernatant through a Ni-NTA column (HisTrap FF; GE Healthcare). The fusion protein was then eluted with elution buffer (NaCl 500 mM, sodium phosphate 40 mM, and imidazole 250 mM, pH 7.0). To remove imidazole, the fusion protein buffer was changed to TN buffer (Tris·HCl 40 mM and NaCl 400 mM, pH 8.0) by centrifugal filtration (Amicon H Ultra; Millipore) at 3,000 × *g* and 4 °C. For fusion protein cleavage, 5 μg of recombinant TEV protease, a gift from Reuven Weiner, The Hebrew University of Jerusalem, Israel, was added per milligram of fusion protein in TEV protease cleavage solution [NaCl 250 mM, Tris·HCl 25 mM, reduced glutathione 0.6 mM, and oxidized glutathione 0.4 mM, pH 7]. The cleavage reaction was performed at room temperature for 22 h. Released toxin was purified via RP-HPLC (C18 column; Phenomenex) using 5–50% gradient of acetonitrile (solution B) in 0.1% TFA in water (solution A) over 45 min. Protein absorbance was monitored at 280 nm, and fractions were manually collected accordingly. Eluted samples were lyophilized and then dissolved in double-distilled water. Fractions were loaded onto SDS/PAGE to detect proteins in the expected size. Positive fractions were further analyzed for activity in TREx HEK293T cells stably expressing rTRPV1 by live-cell calcium imaging and were subjected to mass spectrometry. All protein concentrations were determined by predicted extinction coefficient at 280 nm.

***C. elegans* Strains and Behavioral Assay.** Worm culture and genetics were based on standard procedures (50). WT worms (N2) were obtained from the Caenorhabditis Genetics Center, which is funded by the National Institutes of Health Office of Research Infrastructure Programs (P40 OD010440).

Transgenic strains were obtained using the MosSCI method (51): COP1493, *knuSi749 [pnu1336(Posm10::rtrpv1-wt-(codon-optimized)::2xlinker(introned)::tbb-2u, unc-119(+))] II; unc-119(ed3) III; osm-9(ky10) IV; rtIs27 (Posm-10::GFP X)* and COP1792, *knuSi784 [pnu1336(Posm10::rtrpv1-Δ23-(codon-optimized)::2xlinker(introned)::tbb-2u, unc-119(+))] II; unc-119(ed3) III; osm-9(ky10) IV; rtIs27 (Posm-10::GFP X)*. Behavioral trials were performed by placing a drop containing M13 control buffer (in millimolar: 30 Tris·HCl, pH 7.0, 100 NaCl, and 10 KCl) supplemented with 1% ethanol or toxins in front of a moving worm as previously described (52). Briefly, young adults were transferred from *Escherichia coli* OP50-containing nematode growth media plates to plates without food. The behavioral assay was performed after 15 min of transfer. Agonists included capsaicin (Tocris Bioscience) and WT and mutant DkTx. For sensitization assays, worms were incubated for 15 min in M13 with 5 μM DkTx before a capsaicin challenge.

DkTx Mutagenesis. The plasmid pLic-MBP-DkTx was a kind gift from Glenn F. King, The University of Queensland, Brisbane, Australia. Mutated DkTx genes were produced by overlap PCR techniques (New England Biolabs), as previously described (53). K1 was produced by introducing a stop codon and HindIII restriction site to the end of K1 of DkTx. K2 was produced by introducing an Acc65I restriction site to the start of K2. K1K1 was produced by introducing an MfeI restriction site to the start of K1 and a stop codon and HindIII restriction site to its end. K2K2 was produced by introducing an Acc65I restriction site to the start of K2 and MfeI restriction site to its end. DkTx(DL) was produced by introducing seven glycines to the middle of the DkTx's linker. The obtained genes were cloned into pLic-MBP-DkTx using HindIII, Acc65I, and/or MfeI restriction enzymes (New England Biolabs) and T4 DNA ligase (Thermo Scientific) to produce the desired mutated DkTx plasmid. All DNA constructs were sequenced (Hy Laboratories) to verify successful mutagenesis.

TRPV1 Mutagenesis. TRPV1Δ23 was generated by deleting the channel pore turret (604–626) using the Gibson assembly method. Briefly, the TRPV1 fragments N-terminal-603 and 627-C-terminal were produced by overlap PCR techniques (New England Biolabs) with primers (Sigma) designed using the NEBuilder assembly tool software (New England Biolabs). Using the Gibson assembly master mix (New England Biolabs), fragments were then assembled and cloned into a pcDNA4/TO vector that was previously cleaved by HindIII and ApaI. The artificial turret TRPV1 channel was generated by insertion of a sequence ($G_4SG_4SG_4SG_4SGSG$) after the 603 position in the TRPV1Δ23 pcDNA4/TO construct using the Q5 Site-directed Mutagenesis Kit (New England Biolabs) according to the manufacturer's protocol. Site-directed mutagenesis of the wt rTRPV1 gene cloned into a pCDNA4/TO plasmid was performed by overlap PCR techniques using Phusion High-Fidelity DNA Polymerase (New England Biolabs). Following digestion with the restriction enzymes HindIII and ApaI, 3P-A turret TRPV1 was subcloned into the pCDNA4/TO plasmid using the T4 DNA ligase (Thermo Scientific), according to the manufacturer's protocol. All constructs were verified by sequencing (Hy Laboratories).

Cell Culture. Cells were cultured as previously described (11). rTRPV1 was stably expressed in TREx 293 cells following the manufacturer's protocol (Invitrogen). Briefly, TREx host cell line (Invitrogen) was transfected with pcDNA4/TO containing the gene of interest using Mirus LT1 transfection reagent (Mirus Bio). Successful recombination and maintenance of the rTRPV1 gene were confirmed through zeocin (500 μg/mL; Invivogen) selection to establish a stably transfected cell line. rTRPV1 TREx 293 cells were grown in DMEM (Sigma-Aldrich) supplemented with 10% FBS, 1% penicillin–streptomycin, 500 μg/mL zeocin, 5 μg/mL blasticidin, 2 mM L-alanine L-glutamine, and 25 mM Hepes (pH 7.3). rTRPV1 and mutated channels were transiently expressed in CHO cells or TREx 293 cells following the manufacturer's protocol. CHO cells were grown in F12 medium supplemented with 10% FBS and 1% penicillin–streptomycin. Cells were grown at 37 °C and 5% CO_2 and were passed twice a week.

Electrophysiology. Whole-cell configuration of the patch-clamp technique was performed as previously described (53). Briefly, rTRPV1 TREx 293 cells were plated onto glass coverslips (12 mm) coated with 0.1 mg/mL poly-D-lysine (PDL; Sigma-Aldrich) 16 h before recordings. rTRPV1 expression was induced with 1 μg/mL doxycycline (Sigma-Aldrich) 3 h before recordings. Patch electrodes were pulled from borosilicate glass using the P1000 Micropipette Puller (Sutter Instrument) and fire-polished to a resistance of 2–4 MΩ using microforge MF-900 (Narishige). Membrane currents were recorded under the voltage clamp using an Axopatch 200B patch-clamp amplifier (Molecular Devices), digitized using a Digidata 1440A interface board and pCLAMP 10.6 software (Molecular Devices) with sampling frequency set to 10 kHz and low-pass-filtered at 2 kHz. Currents were recorded using a ramp protocol (−80 mV to +80 mV) to analyze the rectification of TRPV1 currents. The extracellular solution contained (in millimolar) 140 NaCl, 2.8 KCl, 2 $MgSO_4$, 5 Hepes, and 5 MES and was adjusted to pH 7.4 with NaOH. The pipette solution contained (in millimolar) 140 CsCl, 2.8 KCl, 5 MES, 2 $MgSO_4$, and 5 Hepes adjusted to pH 7.4 with CsOH. Calcium was excluded from solutions to avoid Ca^{2+}-dependent TRPV1 desensitization (6, 54). For toxin and drug application, extracellular solutions were applied by the microperfusion system μFlow (ALA Scientific Instruments). All experiments were carried out at room temperature.

Single-channel currents were recorded in the outside-out patch configuration of the patch-clamp technique, as previously described (53). Cell plating and rTRPV1 expression induction were performed as described above. Electrodes were pulled and fire-polished to a resistance of 10–25 MΩ. Patch electrodes were coated with Sylgard (World Precision Instrument). Single-channel currents were low-pass-filtered at 2 kHz or 5 kHz and digitized at 20 kHz. Currents were recorded at a holding voltage of +60 mV. For the single-channel current–voltage relation experiment, a voltage step protocol (−80 mV to +80 mV) was used. Extracellular solution was the same used for whole-cell recordings. The pipette solution contained (in millimolar) 150 sodium gluconate, 15 NaCl, 5 EGTA, and 10 Hepes adjusted to pH 7.4 with NaOH. Drug application was performed as described above. All experiments were carried out at room temperature. For presentation, traces were digitally filtered at 1 kHz.

Ratiometric Calcium Imaging. Live-cell calcium imaging was performed as previously described (11, 16). Briefly, rTRPV1 TREx 293 cells were spotted onto glass coverslips (15 mm) coated with 0.2 mg/mL PDL and allowed to settle down for 30 min at 37 °C and 5% CO_2. Then, rTRPV1 expression was induced with 1 μg/mL doxycycline for 3 h. Cells were washed with Ringer solution (in millimolar): 150 NaCl, 2.5 KCl, 1.8 $CaCl_2$,1 $MgSO_4$, 10 Hepes, and 10 D-glucose, adjusted to pH 7.4 with NaOH. Cells were loaded with 3 μM Fura-2-AM (Biotium) dissolved in Ringer solution and supplemented with Pluronic F-127 acid (0.02%; Sigma-Aldrich) for 1 h at room temperature in the dark. Cells were then washed twice with Ringer solution and incubated at room temperature in the dark for 30 min. Ringer solution and drugs were applied using the SPK-8 perfusion system connected to a VC3 controller (ALA Scientific Instruments), while toxins were added directly to the recording chamber. To test heat response, solutions were passed through SC-20 in-line solution heater (Warner Instruments). Cells were illuminated with a 175-W xenon arc lamp, and excitation wavelengths (340/380 nm) were selected by a Lambda DG-4 monochromatic wavelength changer (Sutter Instrument). Intracellular Ca^{2+} concentration was measured by digital video microfluorometry with a front-illuminated interline CCD camera (Exi Blue; QImaging) using MetaFluor Fluorescence Ratio Imaging Software (Molecular Devices). Dual images (340- and 380-nm excitation, 510-nm emission) were collected, and pseudocolor ratiometric images were monitored every 4 s during the experiment. All experiments were conducted at room temperature.

Structural Modeling. Models of TRPV1 including the pore turret were constructed using the loop modeling application of ROSETTA (35), on the basis of the high-resolution cryo-EM structure of rTRPV1 (with deletions in the N and C termini, and at the S5-pore helix loop, Δ23) with RTX and DkTx bound (Protein Data Bank ID code 5IRX) (24). Two cases were examined: one with intact DkTx and another in which the linker was deleted. For each case, 4,000 all-atom models were generated using the Kinematic Closure method (55). The four pore turrets were modeled one by one, sequentially. The protein fragment modeled comprised residues 600–626 (i.e., the 600–604 fragment in the cryo-EM structure of rTRPV1 was remodeled). It was assumed, therefore, that the hydrophobic contacts of I599 and T627 within the proposed temperature-sensing region (21) are shared by rTRPV1 cryo and WT rTRPV1. Elsewhere (residues 335–599 and 627–751), the backbone of the protein was unchanged, and side chains were remodeled only if found within 10 Å of a modeled turret. Each model was scored using the ROSETTA energy function, including terms specific for membrane-protein modeling (56). For the models based on the rTRPV1 cryo/DkTx complex, a second score was introduced to exclude models whereby the pore turrets added to the two-channel subunits underneath DkTx are more peripheral than the toxin linkers (i.e., more than 40% of the Cα atoms in the turret are >19 Å from the center of the pore). The top-ranking 200 models were selected for graphical representation and further analysis. Specifically, for each model, a pore-radius profile was calculated using HOLE (57), and the resulting profiles were averaged for each set.

Data Analysis. All statistical data were calculated using SigmaPlot 11 (Systat Software) and Prism 7 (GraphPad Software) software. For electrophysiology and *C. elegans* behavior, Student's *t* test, ANOVA, and Wilcoxon matched-pairs signed rank tests were used to determine statistical significance. The asterisks indicate values significantly different from experimental control: $***P < 0.001$, $**P < 0.01$, and $*P < 0.05$.

For worms' behavioral data, the Boltzmann equation was used to fit the dose–response data. Dose–responses were calculated using the sigmoidal Hill equation as follows:

$$I \Big/ I_{max} = \frac{[x]^n}{EC_{50}{}^n + [x]^n},$$

where I = measured current, I_{max} = maximal current at the relevant saturating dose (premeasured for each construct), x = tested agonist concentration, EC_{50} = calculated concentration that elicits 50% of maximal current, and n = Hill coefficient. Clampfit 10.6 software (Molecular Devices) was used for single-channel analysis. For each construct, 300–1,400 events were collected from 4 to 16 separate outside-out patches. To determine channel amplitude, all-point amplitude histograms were generated using data digitally filtered at 2 kHz or 5 kHz (53). Traces were idealized using the half-amplitude threshold crossing method and QuB Software (53, 58).

ACKNOWLEDGMENTS. We thank the A.P. laboratory members for insightful comments and Dr. J. F. Cordero-Morales for experimental advice and critically reading the manuscript. This work was supported by a start-up research grant from the United States–Israel Binational Science Foundation (Grant 2015221, to V.V. and A.P.), American Heart Association Grant 16SDG26700010 (to V.V.), Israel Science Foundation Grant 1444/16 (to A.P.), a Paula Goldberg fellowship (to M.G.), and a Jerusalem Brain Committee Postdoctoral Fellowship (to R.K.). W.Z. and J.D.F.-G. are funded by the Intramural Research Program of the National Heart, Lung and Blood Institute, NIH. This work was carried out in part with resources from the NIH Supercomputer Biowulf.

1. Bohlen CJ, Julius D (2012) Receptor-targeting mechanisms of pain-causing toxins: How ow? *Toxicon* 60:254–264.
2. Kalia J, et al. (2015) From foe to friend: Using animal toxins to investigate ion channel function. *J Mol Biol* 427:158–175.
3. Trim SA, Trim CM (2013) Venom: The sharp end of pain therapeutics. *Br J Pain* 7: 179–188.
4. Chacur M, et al. (2004) Snake venom components enhance pain upon subcutaneous injection: An initial examination of spinal cord mediators. *Pain* 111:65–76.
5. Harris JB, Scott-Davey T (2013) Secreted phospholipases A2 of snake venoms: Effects on the peripheral neuromuscular system with comments on the role of phospholipases A2 in disorders of the CNS and their uses in industry. *Toxins (Basel)* 5:2533–2571.
6. Caterina MJ, et al. (1997) The capsaicin receptor: A heat-activated ion channel in the pain pathway. *Nature* 389:816–824.
7. Cao E, Cordero-Morales JF, Liu B, Qin F, Julius D (2013) TRPV1 channels are intrinsically heat sensitive and negatively regulated by phosphoinositide lipids. *Neuron* 77: 667–679.
8. Vriens J, Appendino G, Nilius B (2009) Pharmacology of vanilloid transient receptor potential cation channels. *Mol Pharmacol* 75:1262–1279.
9. Min JW, Liu WH, He XH, Peng BW (2013) Different types of toxins targeting TRPV1 in pain. *Toxicon* 71:66–75.
10. Jordt SE, Tominaga M, Julius D (2000) Acid potentiation of the capsaicin receptor determined by a key extracellular site. *Proc Natl Acad Sci USA* 97:8134–8139.
11. Kumar R, et al. (2017) Activation of transient receptor potential vanilloid 1 by lipoxygenase metabolites depends on PKC phosphorylation. *FASEB J* 31:1238–1247.
12. Siemens J, et al. (2006) Spider toxins activate the capsaicin receptor to produce inflammatory pain. *Nature* 444:208–212.
13. Bohlen CJ, et al. (2010) A bivalent tarantula toxin activates the capsaicin receptor, TRPV1, by targeting the outer pore domain. *Cell* 141:834–845.
14. Yang S, et al. (2015) A pain-inducing centipede toxin targets the heat activation machinery of nociceptor TRPV1. *Nat Commun* 6:8297.
15. Hakim MA, et al. (2015) Scorpion toxin, BmP01, induces pain by targeting TRPV1 channel. *Toxins (Basel)* 7:3671–3687.
16. Geron M, et al. (2017) Protein toxins of the Echis coloratus viper venom directly activate TRPV1. *Biochim Biophys Acta Gen Subj* 1861:615–623.
17. Chou MZ, Mtui T, Gao Y-D, Kohler M, Middleton RE (2004) Resiniferatoxin binds to the capsaicin receptor (TRPV1) near the extracellular side of the S4 transmembrane domain. *Biochemistry* 43:2501–2511.
18. Yang F, et al. (2015) Structural mechanism underlying capsaicin binding and activation of the TRPV1 ion channel. *Nat Chem Biol* 11:518–524.
19. Steinberg X, Lespay-Rebolledo C, Brauchi S (2014) A structural view of ligand-dependent activation in thermoTRP channels. *Front Physiol* 5:171.
20. Yang F, et al. (2018) The conformational wave in capsaicin activation of transient receptor potential vanilloid 1 ion channel. *Nat Commun* 9:2879.
21. Bae C, et al. (2016) Structural insights into the mechanism of activation of the TRPV1 channel by a membrane-bound tarantula toxin. *eLife* 5:e11273.
22. Liang S (2004) An overview of peptide toxins from the venom of the Chinese bird spider Selenocosmia huwena Wang [=Ornithoctonus huwena (Wang)]. *Toxicon* 43: 575–585.
23. Cao E, Liao M, Cheng Y, Julius D (2013) TRPV1 structures in distinct conformations reveal activation mechanisms. *Nature* 504:113–118.
24. Gao Y, Cao E, Julius D, Cheng Y (2016) TRPV1 structures in nanodiscs reveal mechanisms of ligand and lipid action. *Nature* 534:347–351.
25. Bae C, et al. (2012) High yield production and refolding of the double-knot toxin, an activator of TRPV1 channels. *PLoS One* 7:e51516.
26. Jara-Oseguera A, Bae C, Swartz KJ (2016) An external sodium ion binding site controls allosteric gating in TRPV1 channels. *eLife* 5:e13356.
27. Tobin DM, et al. (2002) Combinatorial expression of TRPV channel proteins defines their sensory functions and subcellular localization in C. elegans neurons. *Neuron* 35: 307–318.
28. Kahn-Kirby AH, et al. (2004) Specific polyunsaturated fatty acids drive TRPV-dependent sensory signaling in vivo. *Cell* 119:889–900.
29. Goodman M (2006) Mechanosensation. *WormBook,* 1–14.
30. Julius D (2013) TRP channels and pain. *Annu Rev Cell Dev Biol* 29:355–384.
31. Liao M, Cao E, Julius D, Cheng Y (2013) Structure of the TRPV1 ion channel determined by electron cryo-microscopy. *Nature* 504:107–112.
32. Bootman MD, Rietdorf K, Collins T, Walker S, Sanderson M (2013) Ca2+-sensitive fluorescent dyes and intracellular Ca2+ imaging. *Cold Spring Harb Protoc* 2013:83–99.
33. Yang F, Cui Y, Wang K, Zheng J (2010) Thermosensitive TRP channel pore turret is part of the temperature activation pathway. *Proc Natl Acad Sci USA* 107:7083–7088.
34. Cui Y, et al. (2012) Selective disruption of high sensitivity heat activation but not capsaicin activation of TRPV1 channels by pore turret mutations. *J Gen Physiol* 139: 273–283.
35. Das R, Baker D (2008) Macromolecular modeling with rosetta. *Annu Rev Biochem* 77: 363–382.
36. Elokely K, et al. (2016) Understanding TRPV1 activation by ligands: Insights from the binding modes of capsaicin and resiniferatoxin. *Proc Natl Acad Sci USA* 113:E137–E145.
37. Zheng J (2013) Molecular mechanism of TRP channels. *Compr Physiol* 3:221–242.
38. Winter Z, et al. (2013) Functionally important amino acid residues in the transient receptor potential vanilloid 1 (TRPV1) ion channel–An overview of the current mutational data. *Mol Pain* 9:30.
39. Grandl J, et al. (2010) Temperature-induced opening of TRPV1 ion channel is stabilized by the pore domain. *Nat Neurosci* 13:708–714.
40. Yang F, Ma L, Cao X, Wang K, Zheng J (2014) Divalent cations activate TRPV1 through promoting conformational change of the extracellular region. *J Gen Physiol* 143: 91–103.
41. Velisetty P, Stein RA, Sierra-Valdez FJ, Vásquez V, Cordero-Morales JF (2017) Expression and purification of the pain receptor TRPV1 for spectroscopic analysis. *Sci Rep* 7:9861.
42. Kitaguchi T, Swartz KJ (2005) An inhibitor of TRPV1 channels isolated from funnel web spider venom. *Biochemistry* 44:15544–15549.
43. Monastyrnaya M, et al. (2016) Kunitz-type peptide HCRG21 from the sea anemone heteractis crispa is a full antagonist of the TRPV1 receptor. *Mar Drugs* 14:229.
44. Liu B, Yao J, Wang Y, Li H, Qin F (2009) Proton inhibition of unitary currents of vanilloid receptors. *J Gen Physiol* 134:243–258.
45. Nersesyan Y, et al. (2017) Oxytocin modulates nociception as an agonist of pain-sensing TRPV1. *Cell Rep* 21:1681–1691.
46. Geron M, Hazan A, Priel A (2017) Animal toxins providing insights into TRPV1 activation mechanism. *Toxins (Basel)* 9:326.
47. Steinberg X, et al. (2017) Conformational dynamics in TRPV1 channels reported by an encoded coumarin amino acid. *eLife* 6:e28626.
48. Yang S, et al. (2017) A bimodal activation mechanism underlies scorpion toxin-induced pain. *Sci Adv* 3:e1700810.
49. Klint JK, et al. (2013) Production of recombinant disulfide-rich venom peptides for structural and functional analysis via expression in the periplasm of E. coli. *PLoS One* 8:e63865.
50. Brenner S (1974) The genetics of Caenorhabditis elegans. *Genetics* 77:71–94.
51. Frøkjær-Jensen C, Davis MW, Ailion M, Jorgensen EM (2012) Improved Mos1-mediated transgenesis in C. elegans. *Nat Methods* 9:117–118.
52. Hart A (2006) Behavior. *WormBook* 871:1–67.
53. Hazan A, Kumar R, Matzner H, Priel A (2015) The pain receptor TRPV1 displays agonist-dependent activation stoichiometry. *Sci Rep* 5:12278.
54. Koplas PA, Rosenberg RL, Oxford GS (1997) The role of calcium in the desensitization of capsaicin responses in rat dorsal root ganglion neurons. *J Neurosci* 17:3525–3537.
55. Mandell DJ, Coutsias EA, Kortemme T (2009) Sub-angstrom accuracy in protein loop reconstruction by robotics-inspired conformational sampling. *Nat Methods* 6:551–552.
56. Yarov-Yarovoy V, Schonbrun J, Baker D (2006) Multipass membrane protein structure prediction using Rosetta. *Proteins* 62:1010–1025.
57. Smart OS, Neduvelil JG, Wang X, Wallace BA, Sansom MS (1996) HOLE: A program for the analysis of the pore dimensions of ion channel structural models. *J Mol Graph* 14: 354–360, 376.
58. Studer M, McNaughton PA (2010) Modulation of single-channel properties of TRPV1 by phosphorylation. *J Physiol* 588:3743–3756.